Flinders
UNIVERSITY

Accepted Manuscript

Contrast enhancement by multi-level histogram shape segmentation with adaptive detail enhancement for noise suppression

Damian Tohl, Jim S. Jimmy Li

PII: S0923-5965(18)30752-5
DOI: https://doi.org/10.1016/j.image.2018.10.011
Reference: IMAGE 15464

To appear in: *Signal Processing: Image Communication*

Received date : 31 July 2018
Revised date : 5 October 2018
Accepted date : 31 October 2018

Please cite this article as: D. Tohl and J.S.J. Li, Contrast enhancement by multi-level histogram shape segmentation with adaptive detail enhancement for noise suppression, *Signal Processing: Image Communication* (2018), https://doi.org/10.1016/j.image.2018.10.011

Contrast Enhancement by Multi-Level Histogram Shape Segmentation with Adaptive Detail Enhancement for Noise Suppression

Damian Tohl[a], Jim S. Jimmy Li[a,*]

[a]College of Science and Engineering, Flinders University at Tonsley, GPO Box 2100, Adelaide SA, 5001, Australia

Abstract

The usual problems associated with image enhancement include over- and under-enhancement, halo effects at edges and the degradation of the signal-to-noise ratio as the enhancement of details increases. Some of those problems manifest in the background and some in the details of the enhanced image. Our proposed method is to apply different techniques to enhance the background and details separately. For enhancement of the image background, a novel multi-level histogram shape segmentation method which will detect abrupt changes in the histogram is proposed so that regions of intensity values with a similar frequency of occurrence are segmented for individual equalization to avoid over-enhancement. For detail enhancement, a novel adaptive median based enhancement method is applied to the details to avoid over- and under-enhancement while suppressing noise by limiting the degree of enhancement in homogeneous regions. Halo effects due to the over-enhancement of edges are avoided in our proposed method by using an edge preserving filter for the separation of the background and details so that edges are excluded from detail enhancement. It has been shown that our proposed method is able to avoid the usual adverse problems of image enhancement while producing adequate overall enhancement.

Keywords: Contrast enhancement; histogram shape segmentation; histogram equalization; detail separation; guided image filter.

1. Introduction

Histograms give an overview of the image grey level distribution and density, average luminance, contrast and other characteristics of images [1]. Histogram equalization flattens and stretches the dynamic range of a histogram for image contrast enhancement [2] to improve visual perception [3, 4, 5]. However, there are two main problems associated with standard histogram equalization, namely, over- and under-enhancement in different regions of an image. Over-enhancement results in an unnatural appearance and under-enhancement results in a loss of details [6].

To overcome these problems, one approach [2, 7, 8, 9, 10, 11] is by segmentation of the histogram based on its mean or median value to form sub-images and performing histogram equalization on each sub-image independently. Other approaches [12, 13, 14] include the application of a different weight to each sub-image, as an approach to reduce over- and under- enhancement. However, none of those methods can completely avoid over-enhancement due to the fact that histograms are segmented in a manner such that they may include intensity values with a wide range of frequency of occurrence and this may also cause an undesirable effect of under-enhancement in other regions.

Weighted thresholded histogram equalization (WTHE) [6] applies a weight to the probability density function

*Corresponding author: Tel.: +61-8-82015050;
Email addresses: damian.tohl@flinders.edu.au (Damian Tohl), jimmy.li@flinders.edu.au (Jim S. Jimmy Li)

before histogram equalization. A smaller weight is given to intensity values with a high frequency of occurrence and a larger weight is given to intensity values with a low frequency of occurrence. However, adjusting the weights will not totally eliminate over- and under-enhancement as this still inherits similar problems to histogram equalization. WTHE also tries to preserve image brightness by adding the difference of the mean brightness between the original and the equalized images to the final image, but this may cause clipping of the intensity values and reduce the dynamic range of the image.

For the methods which only segment the histogram into two sub-histograms, namely, brightness preserving bi-histogram equalization (BBHE) [10], dualistic sub-image histogram equalization (DSIHE) [11], bi-weighted histogram equalization (BWHE) [14], and minimum mean brightness error bi-histogram equalization (MMBEBHE) [9], these algorithms will only perform well for images with well-defined bimodal distribution of the intensity values. However, most images will not have the characteristics of such a histogram and those methods will not generally produce favourable outcomes. Additional segmentation thresholds are needed to segment the histogram to reduce the over-enhancement problem.

For methods using multiple sub-histograms, namely, local region stretching adaptive contrast enhancement (LRSACE) [15], recursive mean-separate histogram equalization (RMSHE) [2], recursive sub-image histogram equalization (RSIHE) [8], recursively separated and weighted histogram equalization (RSWHE) [12], and histogram modification using bilateral Bezier curve (HMBBC) [16], over-enhancement still cannot be avoided completely as the histograms are not always segmented at appropriate thresholds. In the LRSACE method, the segmentation thresholds are fixed and therefore not adaptable to various types of images. The recursive methods provide multi-level segmentation, but histograms may be segmented at thresholds that will still cause over-enhancement. Moreover, recursive methods are known to be computationally inefficient.

There are some other histogram based enhancement methods which do not rely on segmenting the histograms, such as the automatic contrast enhancement method using reversible data hiding (ACERDH) [17] and the gamma correction based addition histogram modification method (GCAHM) [18]. ACERDH manipulates histogram bins, merging together those with the lowest frequency of occurrence, but this can lead to a loss of details due to the merger of adjacent histogram bins. GCAHM applies gamma correction to the histogram to level out areas with a similar frequency of occurrence before applying histogram equalization, but this may cause inadequate enhancement. Another gamma based technique is the adaptive gamma correction with weighting distribution method (AGCWD) [13, 19, 20] which uses a modified cumulative distribution function as the adaptive gamma value, but this method tends to increase the brightness of an image which can result in over-enhancement.

Another approach is to treat contrast enhancement as an optimization problem to be solved by minimizing a cost function using an S-shaped curve [21, 22, 23, 24]. The robust image contrast enhancement (RICE) [22] is one such method that also uses the idea of saliency preservation to preserve the brightness in images. However, this method is constricted by the need to preserve brightness and will produce inadequate enhancement in some images.

Other contrast enhancement methods that incorporate optimization problems include the BIQME-optimized image enhancement (BOIEM) [25] and the RIQMC-based optimal histogram mapping (ROHIM) [26] methods. BOIEM and ROHIM are focused on optimising the BIQME and RIQMC image quality measures respectively, to produce an output with optimum enhancement. However, BOIEM optimized with big data will sometimes produce inadequate enhancement while the ROHIM optimized images will sometimes be over-enhanced and neither methods allow a user control over the degree of enhancement to produce a desirable output.

For contrast enhancement in the spatial domain, such as spatial entropy-based contrast enhancement in discrete cosine transform (SECEDCT) [27], residual spatial entropy-based contrast enhancement (RSECE) [28] and spatial mutual information and pagerank-based contrast enhancement (SMIRANK) [29], all three methods produce contrast enhancement based on the distribution of spatial locations of intensity levels. However, those methods do not provide any control over the degree of enhancement and in some cases, the degree of enhancement may be inadequate. Both SECEDCT and RSECE methods tackle this inadequacy by increasing the weight to the high frequency components in the frequency domain to improve detail enhancement. However, this method of

detail enhancement will have minimal effect if the details are already lost in the initial global contrast enhancement. On the other hand, the noise level will be raised and halo effects may be produced when the weights to the high frequency components are increased resulting in output images with worse signal-to-noise ratio and halo effects at edges.

For image enhancement methods with intended applications for enhancing low-light images, methods based on the variational retinex model [30, 31] have been recently developed. However, when the input image requires a high degree of enhancement to produce a brighter image, these methods will produce slight halo effects which are visible at edges. Other image enhancement methods based on neural networks [32] require training and are therefore not suitable for real-time processing.

The problems with existing histogram segmentation equalization techniques are that some segments may include intensity values with a wide range of frequency of occurrence resulting in over- and under- enhancement. This motivates the proposal of our multi-level histogram shape segmentation method that can avoid these problems by segmenting the histogram in such a way that regions with a similar frequency of occurrence are grouped together. Methods that provide detail enhancement will not only enhance details but also noise which is most evident in homogeneous regions of an image. By reducing enhancement adaptively in homogeneous regions where there are no details to be enhanced, our proposed method can reduce noise in those regions and improve the signal-to-noise ratio of the image. Furthermore, by separating the edges from the details prior to performing enhancement using an edge-preserving filter, our proposed method will enhance only the details and not the edges so that halo effects at edges can be avoided.

Section 2 describes our proposed enhancement method and the results are presented in Section 3. Section 4 gives the conclusion.

2. Our Proposed Enhancement Method

To prevent over- and under-enhancement in our proposed method, a different enhancement method is applied to the background and details separately. As a guided image filter (GIF)[33] is known to preserve sharp edges, it is used to separate the details from the image background for separate enhancement. For background enhancement, a novel method to resolve the problem of over-enhancement as a result of histogram equalization is proposed by segmenting the histogram of the background at intensities where abrupt changes have occurred so that each segment includes only intensity values with a similar frequency of occurrence and each segment is then equalized independently. For detail enhancement, a novel technique is applied to enhance extracted details separately to a desirable degree by an adaptive method before re-combination with the enhanced background to produce the image output. Furthermore, a novel noise suppression algorithm based on median of absolute deviation from the median (MAD) [34] is built into the enhancement algorithm so that the degree of enhancement in homogeneous regions is reduced in order to suppress the enhancement of noise for the improvement of the signal-to-noise ratio in the output image.

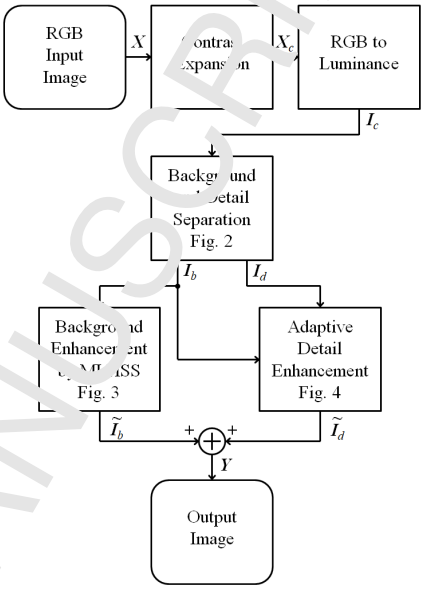

Figure 1: Our proposed overall enhancement method.

An image with a limited range of intensity values will often have poor contrast associated with a limited color dynamic range. Consequently, applying enhancement to the luminance component only will produce an output im-

age with good contrast, but the color of the image will remain dull and faint due to virtually no improvement of the color dynamic range. We therefore, apply the contrast expansion method [21] to the image in the RGB color space to improve the dynamic range of colors as an initial step of our proposed enhancement method.

2.1. Background and Detail Separation

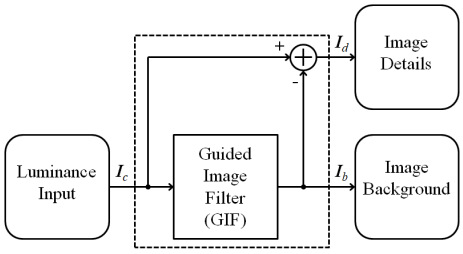

Figure 2: Background and detail separation using a guided image filter.

To extract the background of an image, the conventional method is by filtering the original image by a Gaussian low-pass filter to remove the details. The details are then extracted by taking the difference between the original image and the extracted background [35]. However, this conventional method for detail separation by a Gaussian low-pass filter will include edges in the extracted details and subsequent detail enhancement will cause some degree of halo effects at edges. It is therefore necessary to exclude edges in the extracted details for enhancement. Bilateral [36] and guided image filters (GIF) [33] are known to smooth out details while preserving sharp edges of an image. However, bilateral filters may suffer from "gradient reversal" artefacts [33] and hence, GIF is applied in our proposed method to replace the Gaussian low-pass filter so that the difference between its output and the original image will extract the details without any edges to avoid halo effects as shown in Fig. 2.

Let $\boldsymbol{X}$ be an original image in RGB color space with an intensity range of $[0, L-1]$ where L is 256 for an 8-bit image and $\boldsymbol{X}_c$ is the output processed by the contrast expansion method [21]. Let $\boldsymbol{I}_c$ be the luminance component of $\boldsymbol{X}_c$ and $\boldsymbol{I}_b$ be the image background, which is the GIF output with $\boldsymbol{I}_c$ as the input. Hence, the image details, $\boldsymbol{I}_d$, without containing any edges, can be extracted by the following:

$$\boldsymbol{I}_d = \boldsymbol{I}_c - \boldsymbol{I}_b. \tag{1}$$

The background and details are then enhanced individually.

2.2. Background Enhancement Using Multi-Level Histogram Shape Segmentation

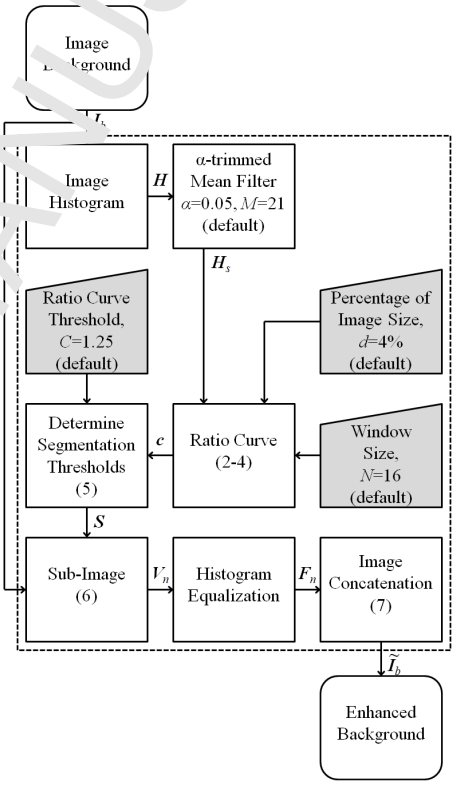

Figure 3: Background enhancement by multi-level histogram shape segmentation with the default values shown for the 807 test images.

In our proposed method, a novel multi-level histogram shape segmentation method is developed for enhancement of the background of the image. In order to avoid over-enhancement, regions of intensity values with a similar

frequency of occurrence have to be separated for processing individually. This can be detected by observing a sudden change in the magnitude of neighbouring values in the histogram of the image background, $\boldsymbol{I}_b$. To prevent small fluctuations and to remove outliers in the histogram from producing an excessive number of segmentation points which will reduce the degree of enhancement, the histogram, H, is smoothed by an α-trimmed mean filter [37] which is known to be able to effectively remove outliers while smoothing the input to produce the output, H_s. A filter window width of $M = 21$ was used for the α-trimmed mean filter and the smallest and largest values inside the filter window were discarded, i.e. $\alpha = 0.05$. Both $M = 21$ and $\alpha = 0.05$ were the default values for all the 807 test images in our experimental results in section 3.

For the detection of abrupt changes at position, q, of the smoothed histogram, H_s, a window on each side of q of width N is formed and the sum of the histogram values inside each window is evaluated, where ${K_q}^l$ and ${K_q}^r$ are the sum of the histogram values inside the windows to the left and right hand side of q respectively as follows:

$$ {K_q}^l = \sum_{k=1}^{N} H_s(q-k), \tag{2} $$

$$ {K_q}^r = \sum_{k=1}^{N} H_s(q+k). \tag{3} $$

This process is repeated for the full range of the histogram to produce a ratio curve, c, which is based on the ratio of the maximum and minimum of ${K_q}^l$ and ${K_q}^r$ as given as follows:

$$ c(q) = \begin{cases} \frac{K_{max}}{K_{min}} & (K_{min} > 0) \,\&\, (K_{max} > (|\boldsymbol{I}_b| \times d)) \\ 1 & otherwise \end{cases}, \tag{4} $$

where $K_{min} = min\left\{{K_q}^l, {K_q}^r\right\}$, $K_{max} = max\left\{{K_q}^l, {K_q}^r\right\}$, $|\boldsymbol{I}_b|$ is the total number of pixels of the background image, $\boldsymbol{I}_b$, d is a percentage of $|\boldsymbol{I}_b|$, and '&' is a logical 'and' operator.

When $K_{min} = 0$ the ratio of K_{max} to K_{min} is undefined at that point and it will be replaced by unity, assuming that it is a flat region in the histogram (i.e. $K_{max} = K_{min}$) at which no abrupt change has occurred. When the number of pixels within the window is too small, i.e. when the number is smaller than a percentage, d, of the size of the image, they are the minority and the ratio should also be ignored and set to unity. The value of d is to be set by the user to control the number of segmentation thresholds in regions of intensity values with a low frequency of occurrence. It is not very critical to the performance of our proposed algorithm and $d = 4\%$ is used as a default value for all the 807 test images in our experimental results in section 3. The peaks of the ratio curve give the location at which abrupt changes of the histogram have occurred and therefore are the locations at which the histogram should be segmented to produce the sub-images. The window width, N, can be used to control the number of peaks in the ratio curve. Increasing N will reduce the number of peaks detected and in turn reduce the number of segmentation thresholds and vice versa. In other words, the degree of enhancement will also be controlled by the value of N. It has been found experimentally that a window size of, $N = 16$, gives the best balance between contrast enhancement and the prevention of over-enhancement for the test images. Hence, $N = 16$ was used as a default value for all the 807 test images in all our experimental results in section 3.

To detect the location of the peaks, the first derivative, c', of the ratio curve is evaluated and the zero-crossings of this derivative give all the peak and trough locations. As only the peak locations are required, only zero-crossings where the sign changes from positive to negative are taken as segmentation thresholds. Let $\boldsymbol{S}$ be the set of the segmentation thresholds located at the peaks of the ratio curve where $n = 1, 2, \ldots, |\boldsymbol{S}|$ and $|\boldsymbol{S}|$ is the cardinal number of $\boldsymbol{S}$ as follows:

$$ \boldsymbol{S} = \{q : (c'(q) > 0) \& (c'(q+1) \leq 0) \& (c(q) > C)\}, \tag{5} $$

where C is a threshold for the slope of the histogram and $N \leq q < L - N$. The range for q is equal to $[N, L-N)$ so that both (2) and (3) are valid.

The ratio curve, $c(q)$ at location q must be greater than the threshold C for an abrupt change of the histogram to have had occurred. In a flat region of the histogram, $c(q) = 1$, hence, C must be greater than unity to detect any abrupt changes. To avoid the inclusion of segmentation thresholds due to minor fluctuations in the histogram, C is set slightly above unity to a value of 1.25. This value of $C = 1.25$ was the default value for all the 807 test images in our experimental results in section 3.

In order to cover the full range of intensity values for an intensity range of $[0, L-1]$, the lower and upper bounds of the intensity range should be included to be the lower and upper segmentation boundaries. Therefore, $S(1) = 0$, $S(|\boldsymbol{S}|) = L$ are added to the set $\boldsymbol{S}$ and all the q values in (5) are re-assigned to $[S(2), \ldots, S(|\boldsymbol{S}|-1)]$ in the ranked-order of magnitude of q. The interval for each sub-image is given by $[S(n), S(n+1)-1]$ where $n = 1, 2, \ldots, (|\boldsymbol{S}|-1)$.

Let $\boldsymbol{V}_n$ be the n^{th} sub-image with intensity values within the intensity interval of $[S(n), S(n+1)-1]$ from the image background, $\boldsymbol{I}_b$ as follows:

$$\boldsymbol{V}_n = \{I_b(i,j) \in \boldsymbol{I}_b : S(n) \leq I_b(i,j) \leq S(n+1)-1\}, \quad (6)$$

where $n = 1, 2, \ldots, (|\boldsymbol{S}|-1)$.

Let $\boldsymbol{F}_n$ be the n^{th} equalized sub-image output of $\boldsymbol{V}_n$ using standard histogram equalization [4]. Each $\boldsymbol{F}_n$ is an equalized sub-image over a section of the full intensity range and the concatenation of all $\boldsymbol{F}_n$ will give an overall equalized background image, $\tilde{\boldsymbol{I}}_b$, with the full intensity range as follows:

$$\tilde{\boldsymbol{I}}_b = \sum_{n=1}^{|\boldsymbol{S}|-1} \boldsymbol{F}_n, \quad (7)$$

where

$$\boldsymbol{F}_n = \{\tilde{I}_b(i,j) \in \tilde{\boldsymbol{I}}_b : S(n) \leq \tilde{I}_b(i,j) \leq S(n+1)-1\}, \quad (8)$$

Fig. 3 gives the block diagram for background enhancement using our proposed multi-level histogram shape segmentation method.

2.3. MAD Based Adaptive Detail Enhancement

A novel median of absolute deviation from the median (MAD) [34] based adaptive method is proposed to enhance only the details to a desirable degree which is settable by a user. In homogeneous regions of an image, there are no details for enhancement and hence, in order to suppress the enhancement of noise to improve the signal-to-noise ratio, no enhancement should be applied in those regions. An adaptive weight to control the degree of enhancement is proposed so that a desirable degree of enhancement will be applied to regions with details while maintaining minimal enhancement in homogeneous regions. The adaptive weight applied to $\boldsymbol{I}_d$ is as follows:

$$\tilde{I}_d(i,j) = w(i,j) I_d(i,j), \quad (9)$$

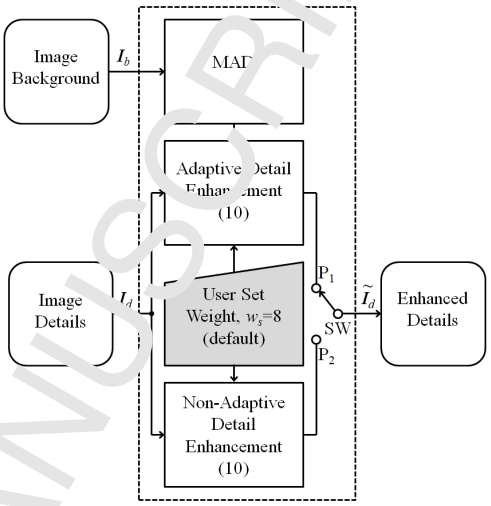

Figure 4: Detail enhancement method with the default values shown for the 8-bit test images. SW is at P_1 when the adaptive algorithm is "ON" and at P_2 when it is "OFF".

where $\tilde{\boldsymbol{I}}_d$ is the enhanced details and $w(i,j)$ is the adaptive weight for detail enhancement at the location (i,j) given as follows:

$$w(i,j) = \begin{cases} w_s + \frac{(1-w_s)}{1+(R\times MAD(i,j))^2} & SW = P_1 \\ w_s & SW = P_2 \end{cases}, \quad (10)$$

where SW is at P_1 when the adaptive algorithm is "ON" and at P_2 when it is "OFF", w_s is the user set weight for detail enhancement, $MAD(i,j)$ is the MAD [34] within a 3x3 filter window centred at (i,j) in the image background, $\boldsymbol{I}_b$, with an intensity range of $[0, L-1]$ and R is a normalized scaler for the MAD given by the following:

$$R = \frac{256}{L}. \quad (11)$$

For 8-bit luminance component, $L = 256$ and $R = 1$.

The MAD is used as a robust estimator for the standard deviation. In homogeneous regions of the image background, $\boldsymbol{I}_b$, the MAD value will tend to zero and therefore the adaptive weight, $w(i,j)$, will tend to unity. In this case, no enhancement will be applied regardless of the value of w_s and hence, there will be no enhancement of

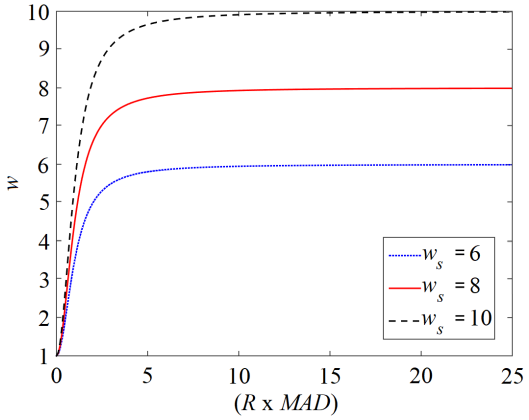

Figure 5: Adaptive weight, w, verses $(R \times MAD)$ for various user set weights, w_s.

noise in those regions for the improvement of the signal-to-noise ratio. In other non-homogeneous regions, the MAD value will be large and the adaptive weight will be approaching the user set weight, w_s. Increasing w_s above unity will increase the degree of detail enhancement in non-homogeneous regions and vice versa. Fig. 5 gives the curves for the adaptive weight, $w(i, j)$, verses $(R \times MAD)$ for different user set weights, w_s by (10). The solid red line, which shows the adaptive weight curve when $SW = P_1$ (i.e. the adaptive algorithm is "ON") and $w_s = 8$, is the default value used for all the 807 test images in our experimental results. When $(R \times MAD)$ tends to zero in homogeneous regions, $w(i, j)$ tends to unity which is the weight for no enhancement. When $(R \times MAD)$ gets larger in non-homogeneous regions, $w(i, j)$ approaches the user set weight quickly, to produce uniform enhancement in all non-homogeneous regions. Fig. 4 gives the block diagram for our proposed MAD based adaptive detail enhancement method. The default position for switch, SW, is P_1, at which adaptive detail enhancement is turned on. However, if the user wishes to enhance weak details in homogeneous regions at the expense of poorer signal-to-noise ratio, the adaptive equation for detail enhancement can be turned off by switching SW to P_2 and the detail enhancement weight, $w(i, j)$, will be a constant value equal to the user set weight w_s for all regions of the image.

The final enhanced image, $\boldsymbol{Y}$, is obtained by combining the enhanced background, $\tilde{\boldsymbol{I}}_b$, with the enhanced details, $\tilde{\boldsymbol{I}}_d$, as follows:

$$\boldsymbol{Y} = \tilde{\boldsymbol{I}}_b + \tilde{\boldsymbol{I}}_d. \tag{12}$$

Refer to Fig. 1 for our proposed overall enhancement method.

3. Results

The test images used for quantitative evaluations and visual assessment are comprised of the TID2013 [38], NIRRGB [39] and CSIQ [40] datasets. The TID2013 dataset [38] consists of 25 reference images for which the contrast is increased and reduced to 5 different levels: "level 1" corresponds to a small contrast reduction; "level 2" corresponds to a small contrast increase; "level 3" corresponds to a larger contrast reduction; "level 4" corresponds to a larger contrast increase; and "level 5" corresponds to the largest contrast reduction. The NIRRGB dataset [39] consists of 477 RGB natural and near-infrared (NIR) images. The CSIQ dataset [40] has 30 reference images to which the contrast is incrementally reduced where "level 1" is the smallest amount of contrast reduction and "level 5" is the largest amount of contrast reduction. All the images from the three datasets, excluding those NIR images in the NIRRGB dataset, giving a total of 807 test images, were used in our tests. These three datasets combined provide a large number of natural and simulated images of varying contrast that provide a significant challenge for many enhancement algorithms.

Our proposed method is compared with ten benchmarking algorithms, namely, RSWHE [12], WTHE [6], AGCWD [13], SSTF [24], RICE [22], SECEDCT [27], SMRIANK [29], BOIEM [25], ROHIM [26] and IESCSA [21]. Default parameter settings for all algorithms are used. In our proposed method, the user set weight for detail enhancement, $w_s = 8$, was used for all our experimental results except Fig. 8 which shows the effect of enhancement with various values of w_s.

3.1. Quantitative Results

Three image quality measures (IQMs), namely, the quality-aware relative contrast measure (QRCM) [29], the blind image quality measure of enhanced images (BIQME) [25] and the no-reference image quality metric

Table 1: The p-values for $QRCM_A > QRCM_B$. M1:RSWHE, M2:WTHE, M3:AGCWD, M4:SSTF, M5:RICE, M6:FCEDCT, M7:SMIRANK, M8:BOIEM, M9:ROHIM, M10:IESCSA, M11:Proposed ($SW{=}P_1$), M12:Proposed ($SW{=}P_2$).

	Alg. B											
Alg. A	M1	M2	M3	M4	M5	M6	M7	M8	M9	M10	M11	M12
M1	-	0.102	0.302	0.193	0.380	0.000	0.001	0.200	0.188	0.069	0.000	0.000
M2	0.898	-	0.606	0.788	0.855	0.002	0.029	0.773	0.439	0.492	0.000	0.000
M3	0.698	0.394	-	0.520	0.682	0.009	0.083	0.[illegible]	0.[illegible]67	0.416	0.019	0.001
M4	0.807	0.211	0.480	-	0.756	0.005	0.031	0.684	0.284	0.317	0.005	0.000
M5	0.617	0.145	0.318	0.243	-	0.002	0.010	0.05[illegible]	0.229	0.102	0.002	0.000
M6	1.000	0.998	0.991	0.995	0.998	-	0.984	0.99[illegible]	0.979	0.989	0.357	0.072
M7	0.999	0.970	0.916	0.969	0.990	0.016	-	0.967	0.813	0.892	0.033	0.005
M8	0.800	0.226	0.379	0.316	0.949	0.002	0.033	-	0.285	0.192	0.002	0.000
M9	0.812	0.560	0.633	0.716	0.771	0.021	0.1[illegible]6	0.715	-	0.515	0.031	0.010
M10	0.929	0.507	0.582	0.682	0.898	0.0[illegible]1	0.1[illegible]8	0.804	0.483	-	0.016	0.009
M11	1.000	1.000	0.981	0.995	0.998	0.642	0.967	0.998	0.969	0.984	-	0.005
M12	1.000	1.000	0.999	1.000	1.000	0.92[illegible]	0.995	1.000	0.990	0.991	0.995	-

Table 2: The p-values for $BIQME_A > BIQME_B$.

	Alg. B											
Alg. A	M1	M2	M3	M4	M5	M6	M7	M8	M9	M10	M11	M12
M1	-	0.055	0.602	0.34[illegible]	0.336	0.232	0.120	0.222	0.152	0.171	0.010	0.051
M2	0.945	-	0.748	0.[illegible]06	0.914	0.716	0.543	0.857	0.444	0.616	0.325	0.305
M3	0.397	0.250	-	0.375	0.361	0.346	0.268	0.340	0.191	0.285	0.188	0.188
M4	0.652	0.090	0.623	-	0.591	0.301	0.196	0.538	0.197	0.171	0.108	0.104
M5	0.663	0.083	0.[illegible]39	0.406	-	0.302	0.192	0.203	0.202	0.176	0.051	0.089
M6	0.767	0.28[illegible]	0.6[illegible]4	0.698	0.696	-	0.252	0.613	0.279	0.353	0.138	0.144
M7	0.879	0.4[illegible]4	0.[illegible]21	0.804	0.808	0.745	-	0.753	0.369	0.520	0.312	0.291
M8	0.777	0.141	0.660	0.461	0.794	0.384	0.244	-	0.243	0.230	0.084	0.118
M9	0.848	0.[illegible]	0.[illegible]09	0.803	0.792	0.719	0.631	0.755	-	0.585	0.477	0.475
M10	0.82[illegible]	0.383	0.711	0.824	0.823	0.647	0.478	0.768	0.415	-	0.263	0.248
M11	0.99[illegible]	0.672	0.812	0.891	0.948	0.862	0.686	0.914	0.522	0.735	-	0.338
M12	0.949	0.[illegible]5	0.810	0.896	0.911	0.856	0.709	0.882	0.523	0.752	0.654	-

Table 3: The p-values for $NIQMC_A > NIQMC_B$.

	Alg. B											
Alg. A	M1	M2	M3	M4	M5	M6	M7	M8	M9	M10	M11	M12
M1	-	0.086	0.437	0.494	0.596	0.089	0.015	0.421	0.284	0.286	0.024	0.009
M2	0.914	-	0.670	0.968	0.901	0.487	0.202	0.890	0.522	0.726	0.393	0.227
M3	0.563	0.330	-	0.606	0.590	0.361	0.222	0.574	0.361	0.512	0.327	0.270
M4	0.506	0.032	0.394	-	0.532	0.046	0.017	0.150	0.094	0.154	0.045	0.016
M5	0.404	0.099	0.410	0.468	-	0.071	0.015	0.230	0.247	0.257	0.026	0.009
M6	0.910	0.512	0.639	0.953	0.929	-	0.140	0.912	0.544	0.838	0.388	0.200
M7	0.985	0.798	0.778	0.983	0.985	0.860	-	0.974	0.699	0.922	0.771	0.585
M8	0.579	0.110	0.426	0.540	0.770	0.088	0.026	-	0.295	0.327	0.037	0.009
M9	0.716	0.478	0.639	0.906	0.753	0.456	0.301	0.705	-	0.672	0.441	0.354
M10	0.714	0.273	0.488	0.846	0.743	0.161	0.078	0.673	0.328	-	0.141	0.050
M11	0.976	0.606	0.673	0.955	0.974	0.612	0.228	0.963	0.559	0.859	-	0.076
M12	0.991	0.773	0.730	0.984	0.991	0.799	0.415	0.991	0.646	0.950	0.924	-

Table 4: The average processing time per image for each algorithm in seconds for each dataset.

	Time in seconds		
Algorithm	TID2013	CSIQ	NIRK B
HE	0.31	0.3	0.79
RSWHE	0.31	0.34	0.78
WTHE	0.37	0.40	0.89
AGCWD	0.34	0.38	0.88
RICE	0.40	0.43	0.95
SECEDCT	1.11	1.10	3.08
SMIRANK	1.05	0.79	2.07
BOIEM	2.88	2.77	4.23
ROHIM	7.09	9.37	24.36
IESCSA	16.58	13.37	14.39
Proposed	2.12	2.16	5.70
Average	2.96	2.86	5.28

for contrast distortion (NIQMC) [41] were used for our quantitative comparison. QRCM is a combination of the relative contrast enhancement between the input and output image, and any distortions that result from enhancement, BIQME combines contrast, sharpness, brightness, colorfulness and naturalness into one quality score using a regression module and NIQMC combines both local and global information together to produce a score based on the concept of information maximization. All the benchmarking and our proposed algorithm were evaluated using all the 807 test images from the three datasets. The QRCM, BIQME and NIQMC values for each benchmarking algorithm were found for each of the 807 test images to statistically determine which algorithm provided the best enhancement.

The p-values [29] in Table 1, represent the proportion of enhanced test images when $\{QRCM_A > QRCM_B\}$ where $QRCM_A$ and $QRCM_B$ are QRCM values produced by algorithms A and B, for a test image, respectively. When compared with all the ten benchmarking algorithms, namely, RSWHE (i.e. M1), WTHE (i.e. M2), AGCWD (i.e. M3), SSTF (i.e. M4), RICE (i.e. M5),

SECEDCT (i.e. M6), SMIRANK (i.e. M7), BOIEM (i.e. M8), ROHIM (i.e. M9), and IESCSA (i.e. M10), our proposed method when the adaptive algorithm was "on" (i.e. Row M11 where SW was at position P_1) produced an average p-value of higher than 0.96 except when compared with SECEDCT (i.e. M6) where it was 0.642. As all the p-values are greater than 0.5, our proposed method when the adaptive algorithm is "on" outperformed all the benchmarking algorithms. When comparing all the ten benchmarking algorithms with our proposed method when the adaptive algorithm was "off" (i.e. Row M12 where SW was at position P_2), the p-values were higher than 0.92 for all the 807 test images. In other words, our proposed algorithm statistically outscored all the ten benchmarking algorithms for all the 807 test images in the three datasets quantitatively regardless of the position of switch, SW. The better score for our proposed method when SW was at position P_2 was due to the fact that QRCM is based on the image gradient and a higher degree of enhancement in the homogeneous regions will give a higher score as a result. On the other hand, the output image when SW is at position P_1 (i.e. the adaptive algorithm is "ON") gives a cleaner image in homogeneous regions as shown in the visual assessment results in the following section 3.2.

For the comparison of our proposed method with the other ten benchmarking algorithms using BLIQME, the p-values in Table 2 show that our proposed method at either position of the switch (i.e. both M11 and M12) outperformed all of the ten benchmarking algorithms with p-values over 0.52.

For the comparison using NIQMC, as shown in Table 3, our proposed method outperformed the other nine benchmarking algorithms except SMIRANK (i.e. M7). One reason is that the NIQMC score is based on the contrast-distortion caused by an enhancement method. As SMIRANK will often over-enhance the contrast of an image, it is not surprising this method produced better results for this IQM. However, its score produced by NIQMC, does not generally agree with the visual assessment as shown in the following visual assessment section.

Table 4 gives the average processing time per image for each algorithm to process the set of test images. All the benchmarking and our proposed algorithms were coded in MATLAB and processed using a Quad Core i7 processor. It shows that the speed of our proposed method is about the average of the speed of all the benchmarking algorithms. Even though our proposed method, when implemented in software using a general purpose processor, is not the fastest among the benchmarking algorithms, its non-iterative structure can be implemented using dedicated hardware, such as field-programmable gate arrays (FPGAs), for real-time processing [42, 43].

3.2. Visual Assessment

Figure 6: The original images used for visual assessment; (a) the *mountain* image, (b) the *lake* image, (c) the *country* image, (d) the *building* image, (e) the *test pattern* image, (f) the *girl* image, (g) the *foxy* image and (h) the *pyramid* image.

In this section, some of the test images from the three datasets, as shown in Fig. 6, were used for visual assessment to compare our proposed method with the ten benchmarking algorithms.

To visually assess our proposed multi-level histogram shape segmentation method for the enhancement of the image background alone, it was only compared with other methods using histogram segmentation, namely, BBHE [10], MMBEBHE [9], RMSHE [2] and RSIHE [8]. In order to clearly illustrate the differences among the methods, cropped regions of the output images are shown with the corresponding histograms in Fig. 7. It is obvious that the whole cropped region, particularly the mountain region at the centre of the image, was over-enhanced with a loss of details by all of the benchmarking algorithms as shown in Fig. 7(b) - Fig. 7(e), while our proposed method produced a better contrast image without any over-enhancement in the sky or mountain regions. It is evident that our proposed method based on the detection of abrupt changes in the histogram was able to avoid the problem of over-enhancement by segmenting the image at appropriate locations of the histogram.

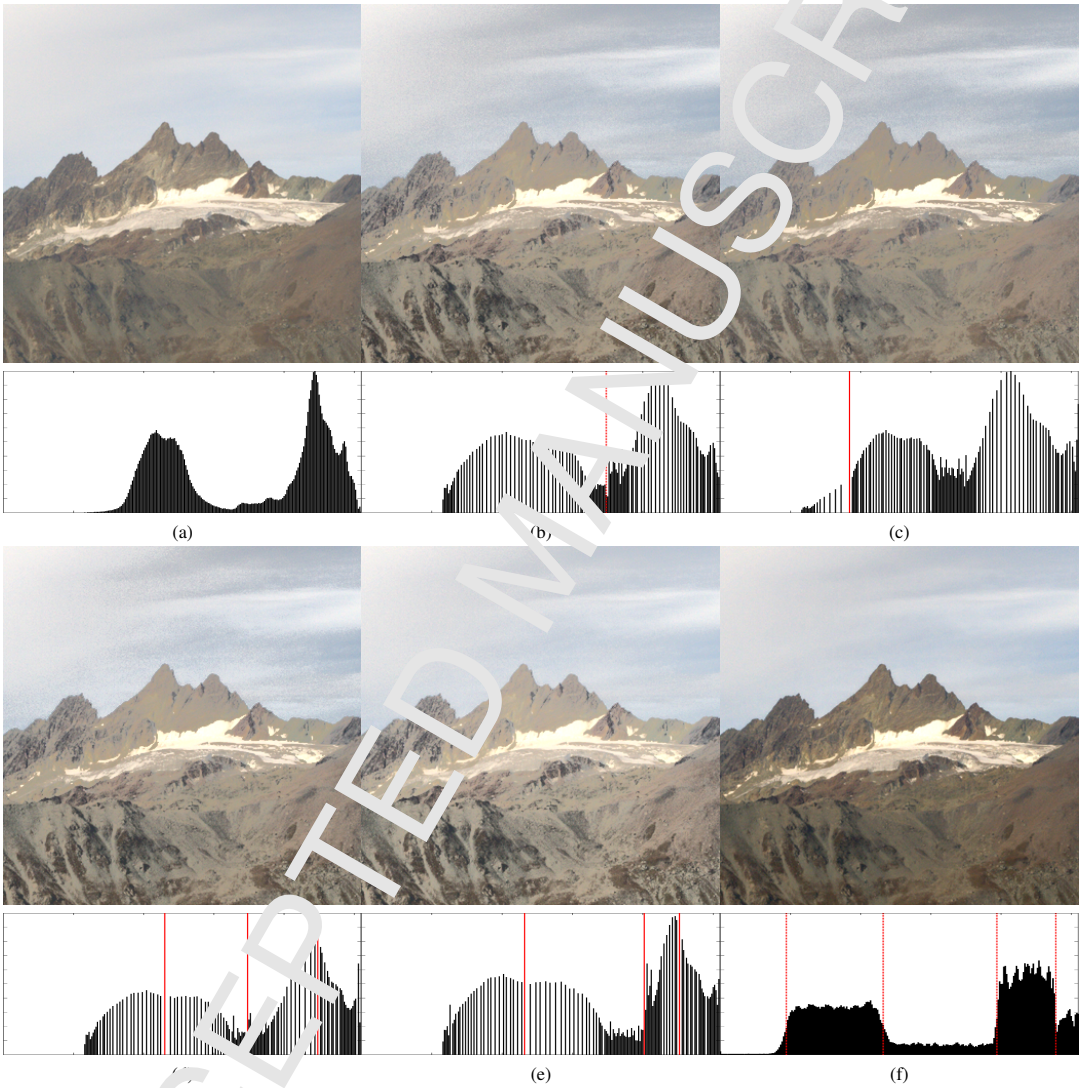

Figure 7: The results of different multi-level histogram equalization methods applied to (a) the *mountain* image from the NIRRGB dataset [39] by (b) BBHE, (c) MMBEBHE, (d) FMSHE, (e) RSIHE, (f) Our proposed method without adaptive detail enhancement (i.e. $w_s = 1$). The red dotted lines in the histograms indicate segmentation locations.

(a) (b)

(c) (d)

Figure 8: The results for our proposed method using a different user set weight, w_s, on (a) the *lake* image from the CSIQ dataset [40] for (b) $w_s = 1$, (c) $w_s = 8$, (d) $w_s = 16$.

(a) (b)

(c) (d)

Figure 9: The results for our proposed method with different guided image filter window sizes on (a) the *country* image from the NIRRGB dataset [39] with (b) [3x3] window size, (c) [5x5] window size, (d) [7x7] window size.

To assess the changes of the degree of detail enhancement with various values of the user set weight, w_s, was set to the values of 1, 8 and 16 as shown in Fig. 8(b) - Fig. 8(d), respectively. This shows that our proposed method allows the user to have control over a wide range of the degree of detail enhancement while most enhancement methods have no or limited control over the degree of detail enhancement. In general, $w_s = 8$, provides a good degree of detail enhancement and hence, it was set as the default value in our experimental results for comparison with other benchmarking algorithms.

To examine the effects of background and detail separation using different window sizes of the GIF, window sizes of 3x3, 5x5 and 7x7 were applied and the output images are shown in Fig. 9(b) - Fig. 9(d), respectively. From our observations, a smaller filter window size will include only finer details while a bigger window size will include more coarse details to be enhanced. In our experimental results, a window size of 5x5 was set as the default value to produce balanced outputs for all our experimental results.

To examine our proposed adaptive detail enhancement algorithm in the suppression of noise in homogeneous regions, the switch SW was set at position P_1 and P_2 to produce the outputs shown in Fig. 11(b) and Fig. 11(c), respectively. When comparing the outputs with the original image, as shown in Fig. 11(a), which is a cropped region of Fig. 6(d), the noise level in the homogeneous region of Fig. 11(b) when the adaptive detail enhancement was turned off (i.e. when $SW = P_2$) was much higher than that in Fig. 11(c) when the adaptive detail enhancement was turned on (i.e. $SW = P_1$). On the other hand, the enhancement in non-homogeneous regions was similar in both Fig. 11(b) and Fig. 11(c).

To examine the difference of the halo effects after detail enhancement between the conventional method using a Gaussian lowpass filter and a GIF for background and detail separation, an image with sharp edges at various angles as shown in Fig. 12(a) was used as the input. The enhanced output produced by the conventional Gaussian lowpass filter, as shown in Fig. 12(b), displayed strong

(a) Input (b) RSWHE (0.034) (c) WTHE (0.052) (d) AGCWD (0.066)

(e) SSTF (0.049) (f) RICE (0.049) (g) SECEDCT (0.174) (h) SMIRANK (0.087)

(i) BOIEM (0.044) (j) ROHIM (0.031) (k) IESCSA (0.059) (l) MLHSS (0.317)

Figure 10: The enhancement results and the corresponding QRCM values (shown in brackets) using (a) the *building* image from the NIRRGB dataset [39] as the input for (b) RSWHE, (c) WTHE, (d) AGCWD, (e) SSTF, (f) RICE, (g) SECEDCT, (h) SMIRANK, (i) BOIEM, (j) ROHIM, (k) IESCSA and (l) Proposed ($SW = P_1$ (i.e. the adaptive algorithm is "ON")).

(a) (b) (c)

Figure 11: The results for different detail enhancement on a cropped area of the (a) the *building* image from the NIRRGB dataset [39] for (b) our proposed method with a constant enhancement weight, $w_s = 8$ (SW at P_2 (i.e. the adaptive algorithm is "OFF")) and (c) our proposed method with adaptive enhancement, $w_s = 8$ (SW at P_1 (i.e. the adaptive algorithm is "ON")).

(a) (b) (c)

Figure 12: The results of using different filter types for background and detail separation on (a) the contrast reduced input image *test pattern* from the TID2013 dataset [38] with (b) a Gaussian low pass filter and (c) a GIF.

halo effects at the proximity of the sharp edges particularly along the rims of the circles and all the characters, while the enhanced output using a GIF as shown in Fig. 12(c), showed no sign of halo effects at all.

For overall visual comparison with other benchmarking enhancement methods, the *building* image, as shown in Fig. 10 from the NIRRGB dataset [39] was used as it consists of sharp edges at different angles of the building and homogeneous regions in the sky and the facade of the building. The benchmarking methods, namely, RSWHE, WTHE, SSTF, RICE, SMIRANK and BOIEM, as shown in Fig. 10(b) - 10(c), Fig. 10(e) - 10(f) and Fig. 10(h) - 10(i) respectively, produced negligible overall enhancement, particularly for the reflections in the window. For AGCWD, ROHIM and IESCSA as shown in Fig. 10(d) Fig. 10(j) and Fig. 10(k) respectively, both produced over-enhanced output images, causing an unnatural appearance in the color of the sky and the building. For the method with separate detail enhancement in the high frequency domain, namely, SECEDCT as shown in Fig.

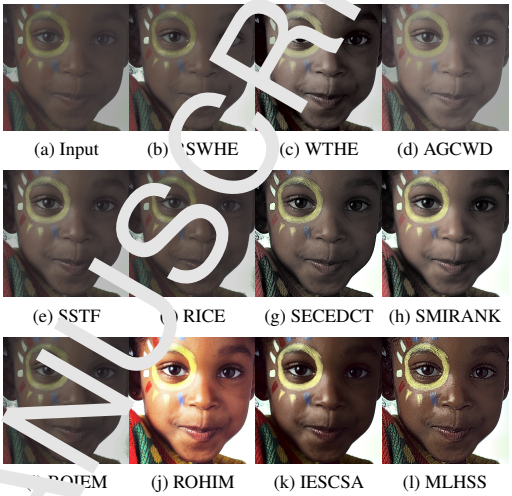

(a) Input (b) RSWHE (c) WTHE (d) AGCWD

(e) SSTF (f) RICE (g) SECEDCT (h) SMIRANK

(i) BOIEM (j) ROHIM (k) IESCSA (l) MLHSS

Figure 13: The enhancement results using (a) the *girl with painted face* image from the TID2013 dataset [38] as the input for (b) RSWHE, (c) WTHE, (d) AGCWD, (e) SSTF, (f) RICE, (g) SECEDCT, (h) SMIRANK, (i) BOIEM, (j) ROHIM, (k) IESCSA and (l) Proposed ($SW = P_1$ (i.e. the adaptive algorithm is "ON")).

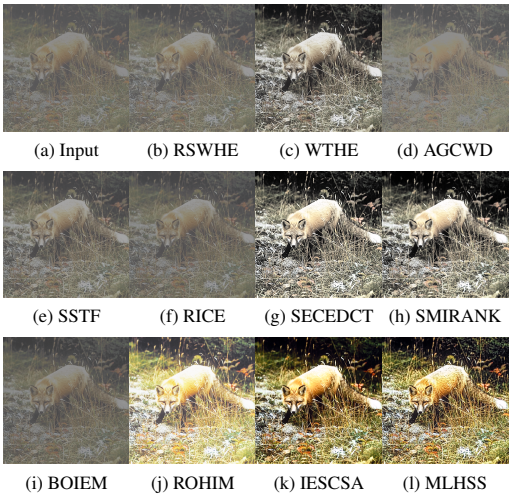

(a) Input (b) RSWHE (c) WTHE (d) AGCWD

(e) SSTF (f) RICE (g) SECEDCT (h) SMIRANK

(i) BOIEM (j) ROHIM (k) IESCSA (l) MLHSS

Figure 14: The enhancement results using (a) the *foxy* image from the CSIQ dataset [40] as the input for (b) RSWHE, (c) WTHE, (d) AGCWD, (e) SSTF, (f) RICE, (g) SECEDCT, (h) SMIRANK, (i) BOIEM, (j) ROHIM, (k) IESCSA and (l) Proposed ($SW = P_1$ (i.e. the adaptive algorithm is "ON")).

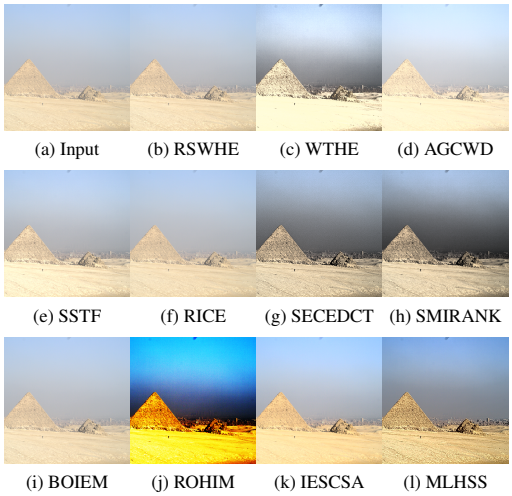

(a) Input (b) RSWHE (c) WTHE (d) AGCWD

(e) SSTF (f) RICE (g) SECEDCT (h) SMIRANK

(i) BOIEM (j) ROHIM (k) IESCSA (l) MLHSS

Figure 15: The enhancement results using (a) the *pyramid* image from the NIRRGB dataset [39] as the input for (b) RSWHE, (c) WTHE, (d) AGCWD, (e) SSTF, (f) RICE, (g) SECEDCT, (h) SMIRANK, (i) BOIEM, (j) ROHIM, (k) IESCSA and (l) Proposed ($SW = P_1$ (i.e. the adaptive algorithm is "ON")).

10(g), halo effects are produced at the edges of the building and noise is also enhanced in the homogeneous regions of the sky and the building facade. Our proposed method was able to enhance the image, particularly the reflections in the window without causing any halo effects and maintain noise free homogeneous regions as shown in Fig. 10(l).

For visual assessment of the enhancement algorithms on natural human skin, which is known to be challenging for many enhancement algorithms, a contrast reduced version of a human face, namely the *girl with painted face* image as shown in Fig. 13(a) was used. The girl's face was over-enhanced by AGCWD with reduced details as shown in Fig. 13(d) and the degree of over-enhancement was even worse for ROHIM as shown in Fig. 13(j), with a loss of details and over-saturation around her right eye and the background. For RSWHE, SSTF, RICE and BOIEM as shown in Fig. 13(b), Fig. 13(e) - 13(f) and Fig. 13(i) respectively, the enhancement methods produced inadequate enhancement with virtually invisible enhancement. For WTHE, SECEDCT, SMIRANK IESCSA, shown in Fig. 13(c), Fig. 13(g) - 13(h) and Fig. 13(k) respectively, the contrast of the girl's face was over-enhanced causing an imbalance of intensity of the girl's face with her left cheek being too dark and her right cheek being too bright. Our proposed method, as shown in Fig. 13(l), gave well balanced enhancement to the background with adequate enhancement of the details. The dynamic range of the color of our proposed method has also been improved and the color has come to life, while the color of most of the other benchmarking algorithms remained dull and faint.

For visual assessment of the enhancement algorithms on a natural scene with wildlife, a contrast reduced version of a fox, namely the *foxy* image as shown in Fig. 14(a) was used. For the benchmarking methods, namely, RSWHE, AGCWD, SSTF, RICE and BOIEM, as shown in Fig. 14(b), Fig. 14(d) - 14(f) and Fig. 14(i) respectively, only minimal enhancement was produced. Stronger enhancement was produced by WTHE, SECEDCT and SMIRANK as shown in Fig. 14(c) and Fig. 14(g) - 14(h) respectively, but the color remains washed out and dull. On the other hand, the enhanced output by ROHIM, as shown in Fig. 14(j), was severely over-enhanced with a loss of details. IESCSA and our proposed method, shown in Fig. 14(k) - 14(l) respectively, both produced strong enhancement with full vivid color, but our proposed method provided sharper detail enhancement, highlighted by the fur coat of the fox.

For visual assessment on a natural landscape, the *pyramid* image as shown in Fig. 15(a) was used. For the benchmarking methods, namely, RSWHE, AGCWD, SSTF, RICE, and BOIEM, as shown in Fig. 15(b), Fig. 15(d) - 15(f) and Fig. 15(i) respectively, inadequate enhancement can be seen in the output images. On the other hand, the WTHE and AGCWD methods, as shown in Fig. 15(c) - 15(d) respectively, over-enhanced the sand in front of the pyramid, resulting in a loss of details. Over-enhancement was also produced by the SECEDCT and SMIRANK methods, as shown in Fig. 15(g) - 15(h) respectively, as seen by the extreme variation of dark and light regions in the sky and the pyramid. ROHIM, as shown in Fig. 15(j), severely over-enhanced the image resulting in highly saturated and unnatural color. IESCSA, as shown in Fig. 15(k) produced some degree of enhancement while our proposed method, as shown in Fig. 15(l) produced adequate natural enhancement revealing more details in the pyramid and the city behind the pyramid.

4. Conclusion

A novel image enhancement method by enhancing the background and details using individual novel enhancement techniques has been proposed. It has been shown that our proposed multi-level histogram shape segmentation method is able to enhance the background of an image without over-enhancement by the segmentation of intensities with a similar frequency of occurrence for individual equalization. By excluding edges in detail enhancement through a guided image filter (GIF), halo effects at edges have been avoided. Our proposed adaptive detail enhancement method was also proven to be able to maintain low noise level in homogeneous regions by suppressing the enhancement of noise in those regions. It has been shown that our proposed method outperformed the other benchmarking algorithms both quantitatively and visually without the usual adverse problems of other enhancement methods in terms of over- and under-enhancement in different regions and halo effects at edges. Future research is the hardware implementation of our proposed method on FPGAs for real-time image enhancement with applications including digital TV.

References

[1] A. Rosenfeld, A. C. Kak, Digital Picture Processing, Academic Press, New York, 1976.

[2] S.-D. Chen, A. R. Ramli, Contrast enhancement using recursive mean-separate histogram equalization for scalable brightness preservation, IEEE Transactions on Consumer Electronics 49 (4) (2003) 1301–1309. doi:10.1109/TCE.2003.1261233.

[3] S. E. Umbaugh, Computer Vision and Image Processing, Prentice Hall, New Jersey, 1998.

[4] R. C. Gonzalez, R. E. Woods, Digital Image Processing, 3rd Edition, Prentice Hall, New Jersey, 2008.

[5] K. R. Castleman, Digital Image Processing, Prentice Hall, New Jersey, 1996.

[6] Q. Wang, R. K. Ward, Fast image/video contrast enhancement based on weighted thresholded histogram equalization, IEEE Transactions on Consumer Electronics 53 (2) (2007) 757–764. doi:10.1109/TCE.2007.381756.

[7] M. H. Kabir, M. Abdullah-Al-Wadud, O. Chae, Brightness preserving image contrast enhancement using weighted mixture of global and local transformation function, Int. Arab J. Inf. Technol. 7 (4) (2010) 403–410.

[8] K. Sim, C. Tso, Y. Tan, Recursive sub-image histogram equalization applied to gray scale images, Pattern Recognition Letters 28 (10) (2007) 1209 – 1221. doi:10.1016/j.patrec.2007.02.003.

[9] S.-D. Chen, A. R. Ramli, Minimum mean brightness error bi-histogram equalization in contrast enhancement, IEEE Transactions on Consumer Electronics 49 (4) (2003) 1310–1319. doi:10.1109/TCE.2003.1261234.

[10] Y.-T. Kim, Contrast enhancement using brightness preserving bi-histogram equalization, IEEE Transactions on Consumer Electronics 43 (1) (1997) 1–8. doi:10.1109/30.580378.

[11] Y. Wang, Q. Chen, B. Zhang, Image enhancement based on equal area dualistic sub-image histogram equalization method, IEEE Transactions on Consumer Electronics 45 (1) (1999) 68–75. doi:10.1109/30.754419.

[12] M. Kim, M. G. Chung, Recursively separated and weighted histogram equalization for brightness preservation and contrast enhancement, IEEE Transactions on Consumer Electronics 54 (3) (2008) 1389–1397. doi:10.1109/TCE.2008.4637632.

[13] S. Huang, F. Cheng, Y. Chiu, Efficient contrast enhancement using adaptive gamma correction with weighting distribution, IEEE Transactions on Image Processing 22 (3) (2013) 1032–1041. doi:10.1109/TIP.2012.2226047.

[14] J. Baby, V. Karunakaran, Bi-level weighted histogram equalization with adaptive gamma correction, International Journal of Computational Engineering Research 4 (3) (2014) 25–30.

[15] S. Srinivasan, N. Balram, Adaptive contrast enhancement using local region stretching, in: The 9th Asian Symposium on Information Display, 2006, pp. 8–12.

[16] F. Cheng, S. Huang, Efficient histogram modification using bilateral bezier curve for the contrast enhancement, Journal of Display Technology 9 (1) (2013) 44–50. doi:10.1109/JDT.2012.2226234.

[17] H.-T. Wu, S. Tang, J. Huang, Y.-Q. Shi, A novel reversible data hiding method with image contrast enhancement, Signal Processing: Image Communication 62 (2018) 64–73. doi:10.1016/j.image.2017.12.006.

[18] X. Wang, L. Chen, An effective histogram modification scheme for image contrast enhancement, Signal Processing: Image Communication 58 (2017) 187–198. doi:10.1016/j.image.2017.07.009.

[19] Y. S. Chiu, F. C. Cheng, S. C. Huang, Efficient contrast enhancement using adaptive gamma correction and cumulative intensity distribution, in: 2011 IEEE International Conference on Systems, Man, and Cybernetics, 2011, pp. 2946–2950. doi:10.1109/ICSMC.2011.6084119.

[20] S. Huang, W. Chen, A new hardware efficient algorithm and reconfigurable architecture for image contrast enhancement, IEEE Transactions on Image Processing 23 (10) (2014) 4426–4437. doi:10.1109/TIP.2014.2349869.

[21] D. Tohl, J. S. J. Li, Image enhancement by s-shaped curves using successive approximation for preserving brightness, IEEE Signal Processing Letters 24 (8) (2017) 1247–1251. doi:10.1109/LSP.2017.2718018.

[22] K. Gu, G. Zhai, X. Yang, W. Zhang, C. W. Chen, Automatic contrast enhancement technology with saliency preservation, IEEE Transactions on Circuits and Systems for Video Technology 25 (9) (2015) 1480–1494. doi:10.1109/TCSVT.2014.2372392.

[23] S. Wang, K. Gu, S. Ma, W. Lin, X. Liu, W. Gao, Guided image contrast enhancement based on retrieved images in cloud, IEEE Transactions on Multimedia 18 (2) (2016) 219–232. doi:10.1109/TMM.2015.2510326.

[24] K. Gu, G. Zhai, M. Liu, X. Min, X. Yang, W. Zhang, Brightness preserving video contrast enhancement using s-shaped transfer function, in: 2013 Visual Communications and Image Processing (VCIP), 2013, pp. 1–6. doi:10.1109/VCIP.2013.6706336.

[25] K. Gu, D. Tao, J. F. Qiao, W. Lin, Learning a no reference quality assessment model of enhanced images with big data, IEEE Transactions on Neural Networks and Learning Systems 29 (4) (2018) 1301–1313. doi:10.1109/TNNLS.2017.2649101.

[26] K. Gu, G. Zhai, W. Lin, M. Liu, The analysis of image contrast: From quality assessment to automatic enhancement, IEEE Transactions on Cybernetics 46 (1) (2016) 284–297. doi:10.1109/TCYB.2015.2401732.

[27] T. Celik, Spatial entropy-based global and local image contrast enhancement, IEEE Transactions on Image Processing 23 (12) (2014) 5298–5308. doi:10.1109/TIP.2014.2364537.

[28] T. Celik, H.-C. Li, Residual spatial entropy-based image contrast enhancement and gradient-based relative contrast measurement, Journal of Modern Optics 63 (16) (2016) 1600–1617. doi:10.1080/09500340.2016.1163427.

[29] T. Celik, Spatial mutual information and pagerank-based contrast enhancement and quality-aware relative contrast measure, IEEE Transactions on Image Processing 25 (10) (2016) 4719–4728. doi:10.1109/TIP.2016.2599103.

[30] S. Park, S. Yu, M. Kim, K. Park, J. Paik, Dual autoencoder network for retinex-based low-light image enhancement, IEEE Access 6 (2018) 22084–22093. doi:10.1109/ACCESS.2018.2812809.

[31] S. Park, B. Moon, S. Ko, S. Yu, J. Paik, Low-light image enhancement using variational optimization-based retinex model, in: 2017 IEEE International Conference on Consumer Electronics (ICCE), 2017, pp. 70–71. doi:10.1109/ICCE.2017.7889233.

[32] K. Park, S. Yu, S. Park, S. Lee, J. Paik, An optimal low dynamic range image generation method using a neural network, IEEE Transactions on Consumer Electronics 64 (1) (2018) 69–76. doi:10.1109/TCE.2018.2811257.

[33] K. He, J. Sun, X. Tang, Guided image filtering, IEEE Transactions on Pattern Analysis and Machine Intelligence 35 (6) (2013) 1397–1409. doi:10.1109/TPAMI.2012.213.

[34] Y. Lee, S. Kassam, Generalized median filtering and related nonlinear filtering techniques, IEEE Transactions on Acoustics, Speech, and Signal Processing 33 (3) (1985) 672–683. doi:10.1109/TASSP.1985.1164591.

[35] T. Luft, C. Colditz, O. Deussen, Image enhancement by unsharp masking the depth buffer, in: International Conference on Computer Graphics and Interactive Techniques (SIGGRAPH), 2006, pp. 1206–1213. doi:10.1145/1179352.1142016.

[36] C. Tomasi, R. Manduchi, Bilateral filtering for gray and color images, in: Sixth International Conference on Computer Vision (IEEE Cat. No.98CH36271), 1998, pp. 839–846. doi:10.1109/ICCV.1998.710815.

[37] J. Bednar, T. Watt, Alpha-trimmed means and their relationship to median filters, IEEE Transactions on Acoustics, Speech, and Signal Processing 32 (1) (1984) 145–153. doi:10.1109/TASSP.1984.1164279.

[38] N. Ponomarenko, L. Jin, O. Ieremeiev, V. Lukin, K. Egiazarian, J. Astola, B. Vozel, K. Chehdi, M. Carli, F. Battisti, C.-C. J. Kuo, Image database tid2013: Peculiarities, results and perspectives, Signal Processing. Image Communication 30 (2015) 57–77. doi:10.1016/j.image.2014.10.009.

[39] M. Brown, S. Ssstrunk, Multi-spectral sift for scene category recognition, in: CVPR 2011, 2011, pp. 177–184. doi:10.1109/CVPR.2011.5995637.

[40] E. C. Larson, D. M. Chandler, Most apparent distortion: full-reference image quality assessment and the role of strategy, Journal of Electronic Imaging 19 (2010) 19 – 19 – 21. doi:10.1117/1.3267105.

[41] K. Gu, W. Lin, G. Zhai, X. Yang, W. Zhang, C. W. Chen, No-reference quality metric of contrast-distorted images based on information maximization, IEEE Transactions on Cybernetics 47 (12) (2017) 4559–4565. doi:10.1109/TCYB.2016.2575544.

[42] D. Bailey, J. S. J. Li, Fpga based multi-shell filter for hot pixel removal within colour filter array demosaicing, in: 2016 International Conference on Image and Vision Computing New Zealand (IVCNZ), 2016, pp. 1–6. doi:10.1109/IVCNZ.2016.7804450.

[43] D. Bailey, S. Randhawa, J. S. J. Li, Advanced bayer demosaicing on fpgas, in: 2015 International Conference on Field Programmable Technology (FPT), 2015, pp. 216–220. doi:10.1109/FPT.2015.7393154.

Ref: IMAGE_2018_625
Title: Contrast Enhancement by Multi-Level Histogram Shape Segmentation with Adaptive Detail Enhancement for Noise Suppression
Journal: Signal Processing: Image Communication

Research Highlights

- Apply different techniques to enhance image background and details separately
- Novel multi-level histogram shape segmentation avoids over-enhancing image background
- Novel adaptive median based detail enhancement reduces noise in homogeneous regions
- Separation of edges from details using an edge-preserving filter avoids halo effects